Astrodynamics Vol. 8, No. 1, 209–220, 2024 https://doi.org/10.1007/s42064-023-0191-3

Lunar orbits for telecommunication and navigation services

Marco Cinelli[1](✉), Emiliano Ortore[2], Giovanni Mengali[3], Alessandro A. Quarta[3], and Christian Circi[4]

1. *Istituto di Astrofisica e Planetologia Spaziali (IAPS), Istituto Nazionale di Astrofisica (INAF), Via del Fosso del Cavaliere 100, Roma 00133, Italy*
2. *School of Aerospace Engineering, Sapienza University of Rome, Via Salaria 881, Rome 00138, Italy*
3. *Department of Civil and Industrial Engineering, University of Pisa, Pisa 56122, Italy*
4. *Department of Astronautical, Electrical, and Energy Engineering, Sapienza University of Rome, Via Salaria 851, Rome 00138, Italy*

ABSTRACT

Orbits that are frozen in an averaged model, including the effect of a disturbing body laying on the equatorial plane of the primary body and the influence of the oblateness of the primary body, have been applied to probes orbiting the Moon. In this scenario, the main disturbing body is represented by the Earth, which is characterized by a certain obliquity with respect to the equatorial plane of the Moon. As a consequence of this, and of the perturbing effects that are not included in the averaged model, such solutions are not perfectly frozen. However, the orbit eccentricity, inclination, and argument of pericenter present limited variations and can be set to guarantee the fulfillment of requirements useful for lunar telecommunication missions and navigation services. Taking advantage of this, a practical case of a Moon-based mission was investigated to propose useful solutions for potential near-future applications.

KEYWORDS

lunar orbits
frozen orbits
lunar telecommunications
lunar navigation services

Research Article

Received: 23 July 2023
Accepted: 30 October 2023

1 Introduction

During the mission lifetime of a spacecraft orbiting a natural satellite of the solar system, the disturbing effect due to the gravitational attraction of the massive body (mother planet), the so-called third-body effect, plays a key role in determining the variation of the orbital parameters of the osculating orbit. In a typical scientific observation mission, high values of orbital inclination (i), which are usually necessary to gain wide latitudinal coverage of a planetary satellite, are often associated with substantial variations in orbit eccentricity (e) [1–3]. In such cases, the pericenter altitude of the spacecraft osculating orbit decreases during the mission, which can eventually cause the vehicle to impact the surface of the planetary satellite in a relatively short time interval. Considering the characteristics of typical science orbits for planetary observations, previous studies [4–6] have highlighted how the time to impact (i.e., the spacecraft lifetime) of a vehicle in a high-inclination orbit is strictly related to the choice of the initial value of the argument of pericenter (ω) of the spacecraft osculating orbit.

In a Moon-based mission scenario, this specific phenomenon occurs at mid and high altitudes, where the third-body effect is important, whereas at low altitudes such a perturbation is not strong enough to generate significant variations in the eccentricity of the osculating orbit. On the other hand, it is well known that Moon-based orbits with mid and high altitudes offer extended Moon surface coverage; thus, they are an important scenario for practical applications, such as orbits that will provide lunar telecommunication and navigation services for near-future missions towards the Earth's natural satellite.

In fact, the Artemis program, with the intention of placing a continuous human presence on the lunar surface, is expected to generate a large amount of

✉ marco.cinelli@uniroma2.it

data to the Moon and from it [7]. In this context, as necessary support for human exploration, it is required to investigate suitable orbits for designing constellations of satellites capable of providing *in situ* communication and navigation services. Therefore, it is important to define a lunar relay constellation concept to provide potential support for (near-future) lunar missions using suitable communication links [8, 9]. In this regard, in Ref. [10] the main requirements to be met by a space communications architecture capable of guaranteeing the Moon's global coverage were defined. These requirements include stable orbits, a small range between an orbiter and a potential lander that operates over the lunar surface, a high average contact duration, a small gap time at all latitudes, and architectural reconfigurability in view of new mission concepts. The resulting "ideal" lunar relay constellation, illustrated in Fig. 1, is made up of three orbits with a 12-h period, that is, a circular orbit in the Moon's equatorial plane and two frozen elliptical orbits with their apsidal lines librating over the lunar north and south poles, respectively. However, other arrangements are possible, and an in-depth review of the available proposals for lunar relay orbiters has been provided by a recent report of the Interagency Operations Advisory Group [11]. Accordingly, the possibility of exploiting scenarios characterized by weak variations in the orbit elements of the probe represents a key factor in designing orbits useful for lunar communication and navigation services. Considering that the variation in e is strictly correlated with that of ω, a (frozen) working orbit with nearly

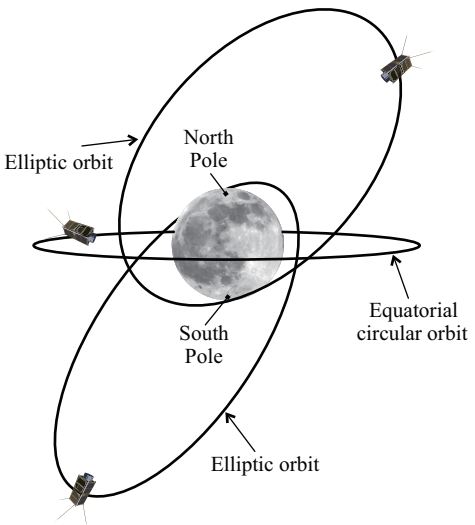

Fig. 1 Conceptual sketch of the "ideal" lunar relay constellation proposed in Ref. [10].

constant values of e and ω would meet this requirement in an optimal manner. In this respect, in Refs. [12] and [13] the problem related to the determination of frozen orbits is addressed considering the zonal harmonics of the gravitational field of the primary body up to J_9 and J_{15}, respectively; in particular, for a probe orbiting the Moon, the interested reader can find in Ref. [14] a thorough discussion on the issue.

In the same context, in Ref. [15] two families of elliptical orbits at constant eccentricity, argument of pericenter, and inclination were proposed. One family is characterized by $\omega = 0$ or 180 deg, and the other by $\omega = 90$ or 270 deg. Note that, in the same reference [15], a third family of polar orbits with $\omega = 0$ or 180 deg and constant values of all the orbit elements has also been found. However, such a specific solution can be considered as a particular case of the one at $\omega = 0$ or 180 deg (obtained when the orbital inclination is 90 deg). These solutions were obtained by exploiting the mean element theory (MET) and considering the effects of both the oblateness of the celestial body around which the spacecraft is orbiting (i.e., the primary) and the gravitational attraction of the disturbing celestial bodies, which are assumed to move on the equatorial plane of the primary. It is well known that the MET is based on an averaged approach, which implies that the orbital elements $\{e, \omega, i\}$ remain constant on average [16–18].

At mid and high altitudes, these two families would meet very well the case of orbits for lunar telecommunication and navigation services. However, as is well known, a Moon-based orbit is characterized by the gravitational perturbations of both the Earth and the Sun, and neither of these two celestial bodies presents a co-planarity condition with the Moon's equatorial plane. In fact, the relative orbits of the Earth and the Sun have obliquities with respect to the Moon's equatorial plane of 6.69 deg and 1.54 deg (= 6.69 − 5.15 deg), respectively, as shown in Fig. 2. However, the values of these obliquity angles are quite small. Therefore, it is expected that the solutions presented in Ref. [15] can be adapted to a Moon-based mission scenario with an acceptable level of approximation. In this way, these solutions will show moderate variations in the orbit elements and will therefore be characterized by long lifetime around the Moon. Following the proposal in Ref. [15], the possibility of exploiting frozen orbits for lunar telecommunication and navigation services is investigated in the present

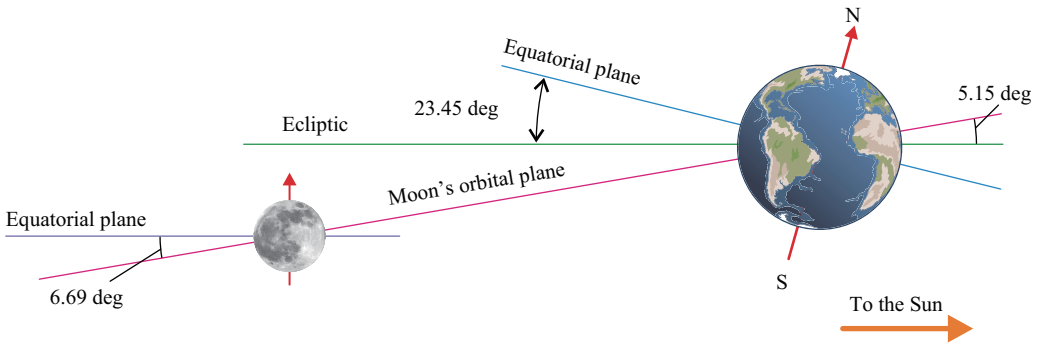

Fig. 2 Relative inclinations of the Earth's and the Moon's equatorial planes. Reproduced with permission from Ref. [19], © Cambridge University Press 2011.

study. Accordingly, in this paper, Section 2 illustrates the mathematical developments necessary for investigating the evolution of the orbit elements of the spacecraft using the MET (under the influence of the oblateness of the primary body and of a third body); then, the two above-mentioned families of frozen orbits are presented. Section 3 explains how the frozen orbits in the averaged model can comply with a Moon-based mission scenario and highlights the advantages of these solutions in terms of probe lifetime. In addition, a numerical analysis considering a non-averaged complete gravitational model is presented, providing results related to a potential lunar mission. Finally, Section 4 summarizes the results of this study.

2 Long-term dynamics and attainment of frozen orbits

The long-term dynamics of a spacecraft orbiting a celestial body, under the disturbing effects arising from the oblateness of the primary body and the gravitational attractions of other celestial bodies, can be studied using the MET. The MET-based procedure consists of first averaging the disturbing function over the orbital periods of both the spacecraft and (disturbing) celestial bodies in their motions around the primary, and then introducing the averaged form of the disturbing function into the classical Lagrange Planetary Equations. The values of the osculating orbit elements of the spacecraft are thus replaced by the mean orbit elements, which is also the assumption used here to study the long-term spacecraft dynamics.

In a Moon-based mission scenario, the main disturbing bodies are the Earth and the Sun. However, considering typical orbits for lunar telecommunication and navigation services, a preliminary numerical analysis of the effects associated with the gravitational attractions of these celestial bodies has shown that the disturbance related to the Sun is very weak compared with that due to the Earth and the Moon's oblateness; therefore, its effect has been removed in the study of the long-term spacecraft dynamics. Accordingly, the aforementioned averages were performed over the orbital periods of the probe and the Earth in their motions about the Moon. Moreover, according to the MET, the orbital elements of the spacecraft osculating orbit and the Earth are assumed to be constant in this average processing, whereas the mean anomalies of the probe (M) and the Earth are averaged out as fast variables (by doing that, M becomes a cyclic variable in the long-term dynamics).

This procedure was conducted by considering the (X, Y, Z) right-handed reference frame illustrated in Fig. 3), whose origin coincides with the Moon's center of mass. The Z axis is aligned with the Moon's polar axis and the X axis is along the nodal line of the Earth's orbit in its apparent motion around the Moon at the initial time instant (i.e., the reference time instant). The plane (X, Y) coincides with the Moon's equatorial plane (the 18.6-year precession of Z around the ecliptic pole E is neglected). Following such a procedure and truncating at second order the traditional expansion in Legendre polynomials of the disturbing function related to the Earth (disturbing body), the long-term equations under the third-body and the Moon oblateness effects can be obtained:

$$\dot{a} = 0 \tag{1}$$

$$\dot{e} = -\frac{15}{16}\frac{\mu_{\mathrm{d}}}{a_{\mathrm{d}}^3(1-e_{\mathrm{d}}^2)^{3/2}}\frac{e\sqrt{1-e^2}}{n}\sin(2\omega)[2\cot(2\omega) \cdot (\sin(2i_{\mathrm{d}})\sin i\sin\Omega - \sin^2 i_{\mathrm{d}}\cos i\sin(2\Omega)) + 2\cos^2(\Omega)$$

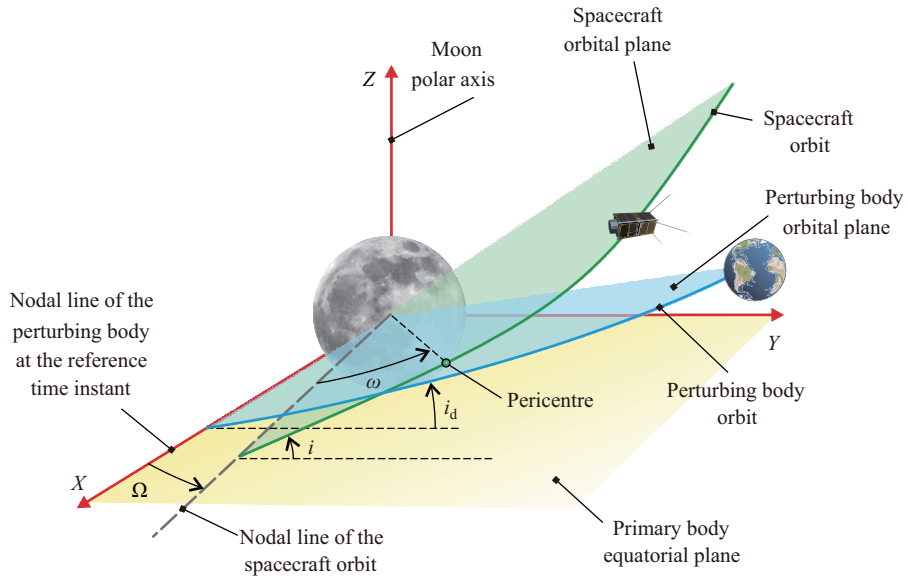

Fig. 3 Lunar reference frame.

$$\cdot (\cos^2 i_\mathrm{d} \cos^2 i - 1) + \sin^2 \Omega(\cos(2i) - \cos(2i_\mathrm{d})) + \sin(2i_\mathrm{d}) \sin(2i) \cos\Omega + 2 \sin^2 i_\mathrm{d} \sin^2 i] \quad (2)$$

$$\dot{i} = \frac{3}{8} \frac{\mu_\mathrm{d}}{a_\mathrm{d}^3 \sqrt{1-e^2}(1-e_\mathrm{d}^2)^{3/2} n} (\sin i_\mathrm{d} \sin i \cos\Omega + \cos i_\mathrm{d} \cos i) \cdot [\sin i_\mathrm{d} \sin\Omega(5e^2 \cos(2\omega) + 3e^2 + 2) + 5e^2 \sin(2\omega)(\sin i_\mathrm{d} \cos i \cos\Omega - \cos i_\mathrm{d} \sin i)] \quad (3)$$

$$\dot{\Omega} = \frac{3\mu_\mathrm{d}}{32 a_\mathrm{d}^3 \sqrt{1-e^2}(1-e_\mathrm{d}^2)^{3/2} n} [\cos i(5e^2 \cos(2\omega) - 3e^2 - 2)(-2 \sin^2 i_\mathrm{d} \cos(2\Omega) + 3\cos(2i_\mathrm{d}) + 1) + 10e^2 \sin(2\omega)(\sin^2 i_\mathrm{d} \sin(2\Omega) + \sin(2i_\mathrm{d}) \cot i \sin\Omega) - 2\sin(2i_\mathrm{d}) \cos(2i) \csc i \cos\Omega(5e^2 \cos(2\omega) - 3e^2 - 2)] - \frac{3J_2 n R_\mathrm{M}^2}{2a^2(1-e^2)^2} \cos i - \dot{\Omega}_\mathrm{d} \quad (4)$$

$$\dot{\omega} = -\frac{3}{128} \frac{\mu_\mathrm{d}}{a_\mathrm{d}^3 \sqrt{1-e^2}(1-e_\mathrm{d}^2)^{3/2} n} \cdot \{4 \sin^2 i_\mathrm{d} \cos(2\Omega)[5(2e^2 - 3)\cos(2\omega) + 6e^2 + 10\cos(2i) \sin^2\omega - 1] + 40(2 - e^2) \sin^2 i_\mathrm{d} \cos i \sin(2\omega) \sin(2\Omega) - 20 \sin(2i_\mathrm{d}) \csc i \sin(2\omega) \sin\Omega[(e^2 - 2)\cos(2i) - 3e^2 + 2] - 4 \sin(2i_\mathrm{d}) \cot i \cos(\Omega) \cdot [2(e^2 - 1)(5\cos(2\omega) - 3) - 20\cos(2i) \sin^2(\omega)] + 2(1 + 3\cos(2i_\mathrm{d}))[5\cos(2\omega)(2e^2 + \cos(2i) - 1) - 2e^2 - 5\cos(2i) - 3]\} + \frac{3J_2 n R_\mathrm{M}^2}{8a^2(1-e^2)^2}(5\cos(2i) + 3) \quad (5)$$

where $\cot\alpha = \cos\alpha/\sin\alpha$ and $\csc\alpha = 1/\sin\alpha$. Moreover, n is the spacecraft mean motion, μ is the Moon's gravitational parameter, J_2 is the first zonal harmonic of the Moon's gravitational field, R_M is the lunar (equatorial) mean radius [20], μ_d is the Earth's gravitational parameter, and $\{a, e, i, \omega\}$ are now the spacecraft mean orbital elements (for simplicity, they have been indicated with the same symbols as the corresponding osculating elements). The parameter Ω was used to indicate the difference between the RAAN of the probe orbit and the RAAN of the Earth's orbit (Ω_d). Note that, since M is a cyclic variable, the semi-major axis is constant on average. The values of the Earth's orbit elements appearing in such a system are reported in Table 1, where $i_\mathrm{d} = 6.69$ deg is the obliquity of the Earth's orbit in the (X, Y, Z) reference frame.

The system described by Eqs. (1)–(5) can be numerically integrated step-by-step to determine the temporal evolution of the mean orbit elements of the probe orbit.

With respect to a previous study on the matter [21], where the RAAN of the disturbing body's orbit was assumed as a constant equal to zero, the temporal derivative of Ω_d now appears as an additional term in Eq. (4). In fact, the assumption that Ω_d is a constant can be made whenever the operational life of the spacecraft is significantly smaller than the rotational period of the nodal line of the perturbing body's orbit. But, in the present scenario, the operational life of the lunar

Table 1 Physical parameters and orbit elements of the Earth in the (X, Y, Z) reference frame

μ	$\mu_{\rm d}$	J_2	$R_{\rm M}$	$a_{\rm d}$	$e_{\rm d}$	$i_{\rm d}$
4902.80 km^3/s^2	398,600.44 km^3/s^2	2.033×10^{-4}	1738 km	384,399 km	0.0549	6.69 deg

probe can be long, making it essential to consider the displacement of the nodal line of the perturbing body's orbit when investigating the spacecraft dynamics (like Z, the perturbing body pole accomplishes a 18.6-year precession around the ecliptic pole E, thus remaining always coplanar with E and Z). Consequently, the system of Eqs. (1)–(5) represents a dynamical model with two and a half degrees of freedom (DOF). In fact, in addition to the two angular coordinates $g = \omega$ and $h = \Omega$ (Delaunay elements), there is also an explicit dependence on the time of $\Omega_{\rm d}$ (non-autonomous system). In particular, the RAAN of the Earth's relative orbit ($\Omega_{\rm d}$) can be assumed to be a linear function of time [22].

2.1 Frozen orbits with a disturbing body on the equatorial plane of the primary body

If the disturbing body moves on the equatorial plane of the primary body (i.e., $i_{\rm d} = 0$), the differential system of Eqs. (1)–(5) simplifies into Eqs. (6)–(10):

$$\dot{a} = 0 \tag{6}$$

$$\dot{e} = \frac{15}{8}\frac{\mu_{\rm d}}{a_{\rm d}^3(1-e_{\rm d}^2)^{3/2}}\frac{e\sqrt{1-e^2}}{n}\sin^2 i \sin(2\omega) \tag{7}$$

$$\dot{i} = -\frac{15}{16}\frac{\mu_{\rm d}}{a_{\rm d}^3(1-e_{\rm d}^2)^{3/2}}\frac{e^2}{n\sqrt{1-e^2}}\sin(2\omega)\sin(2i) \tag{8}$$

$$\begin{aligned}\dot{\Omega} = {} & \frac{3}{8n\sqrt{1-e^2}}\frac{\mu_{\rm d}}{a_{\rm d}^3(1-e_{\rm d}^2)^{3/2}}\cos i(5e^2\cos(2\omega) \\ & - 3e^2 - 2) - \frac{3J_2 n R_{\rm M}^2}{2a^2(1-e^2)^2}\cos i - \dot{\Omega}_{\rm d}\end{aligned} \tag{9}$$

$$\begin{aligned}\dot{\omega} = {} & -\frac{3}{16n}\frac{\mu_{\rm d}}{a_{\rm d}^3\sqrt{1-e^2}(1-e_{\rm d}^2)^{3/2}}[5\cos(2\omega)(2e^2 \\ & + \cos(2i) - 1) - 2e^2 - 5\cos(2i) - 3] \\ & + \frac{3J_2 n R_{\rm M}^2}{8a^2(1-e^2)^2}(5\cos(2i) + 3)\end{aligned} \tag{10}$$

which represents a dynamical model with DOF = 1, where $g = \omega$ is the remaining (single) angular coordinate. In fact, the RAAN of the spacecraft orbit (cyclic variable) does not influence the evolution of eccentricity, inclination, or argument of pericenter; and thus, in practice, a system of three matched equations $\{\dot{e}, \dot{i}, \dot{\omega}\}$ in the three variables $\{e, i, \omega\}$ is obtained. Note that in this (coplanar) case, if the eccentricity is constant on average, the inclination is also constant on average; in fact, these two orbital elements are linked by the well-known Kozai–Lidov equation (which is correlated to the fact that $h = \Omega$ is a cyclic variable) [23–25]:

$$\sqrt{1-e^2}\cos i = C \tag{11}$$

where C is the Kozai–Lidov constant.

For the dynamic model represented by Eqs. (6)–(10), two particular cases can be considered: circular orbits and equatorial orbits. In both cases, the eccentricity and inclination are constant on average.

The behavior of nearly circular orbits was discussed in Ref. [1]. This investigation showed that, under the influence of only the third-body effect, the nearly circular orbits exhibit a stable (non-diverging) behavior of eccentricity if the inclination belongs to the ranges $i <$ 39.43 deg and $i >$ 140.77 deg (which correspond to the so-called third-body critical inclinations); on the contrary, outside these intervals, the eccentricity increases. Then, if the J_2 effect is added, an extension of these zones of stability is obtained.

For the general case of inclined elliptical orbits, in Ref. [15] two families of stationary solutions for $\{\dot{e}, \dot{i}, \dot{\omega}\}$ were obtained. For these two families, the correlation between the values of eccentricity (which is constant on average) and inclination (also constant on average) is given, respectively, by Eqs. (12) and (13) [15]:

$$i = \arccos\left(\sqrt{\frac{1}{5} - \frac{4}{5}(1-e^2)^{5/2}\frac{\omega_{\rm d}}{\omega_0}}\right) \tag{12}$$

$$i = \arcsin\left(\sqrt{\frac{4(1-e^2)^{-2}\omega_0 + [10e^2(1-e^2)^{-1/2} + 4(1-e^2)^{1/2}]\omega_{\rm d}}{5(1-e^2)^{-2}\omega_0 + 10(1-e^2)^{-1/2}\omega_{\rm d}}}\right) \tag{13}$$

More specifically, for the first family, defined by Eq. (12), we have $\omega = 0$ or 180 deg; for the second family, identified by Eq. (13), we have $\omega = 90$ or 270 deg. In such equations, $\omega_{\rm d} = \frac{3}{4}\frac{\mu_{\rm d}}{n a_{\rm d}^3(1-e_{\rm d}^2)}^{3/2}$ and $\omega_0 = \frac{3}{2}\frac{J_2 R_{\rm M}^2 n}{a^2}$ are the parameters associated with the third body and the oblateness, respectively (note that as the orbit altitude increases, the effect of the third body increases, whereas that related to the oblateness decreases).

The frozen orbits given by Eqs. (12) and (13) represent the equilibrium points of the dynamical system with

DOF = 1. These equilibrium points are stable and can be identified as resonance centers in the phase space (ω, e) [6, 23–25].

3 Orbital solutions in a Moon-based mission scenario

As discussed in Section 1, for a probe orbiting the Moon, the hypothesis of coplanarity (assumed in Ref. [15]) between the orbital plane of the disturbing body (the Earth) and the equatorial plane of the Moon is not verified. However, the obliquity of the Earth is quite small (6.69 deg) and therefore it is expected that the results obtained in Ref. [15] (Eqs. (12) and (13)) can be extended to a Moon-based mission scenario with satisfactory accuracy.

Accordingly, Fig. 4 presents the solutions of Eq. (12) (left-hand side plots, hereafter referred to as Fig. 4(a)) and Eq. (13) (right-hand side plots, hereafter referred to as Fig. 4(b)) for a probe orbiting the Moon (note that the Earth's orbit is set here at a null obliquity). The values of the semi-major axis are normalized with respect to the radius of the Moon. Several values of orbit eccentricity have been reported, starting from 0.1, with a step of 0.1. In both figures, the curves consider the collision condition obtained when the radius of the pericenter, $a(1-e)$, becomes equal to the mean radius of the Moon. Therefore, only physically acceptable values are reported in such figures (when the eccentricity increases, the plotted curves reduce their extension accordingly).

The solutions are symmetrical with respect to the case of polar orbit (upper and lower plots). In particular, in the family at $\omega = 0$ or 180 deg, the curves are characterized by high inclinations; moreover, for a fixed value of inclination, the eccentricity increases with the orbit altitude to reach the limit value of 0.47876, in line with Ref. [14]. For the family at $\omega = 90$ or 270 deg, although no theoretical limits for the eccentricity exists, a practical upper limit of 0.7 has been fixed (in this range, the solutions are not associated with high inclinations).

3.1 Results in the averaged model

To determine the lifetime of a probe around the Moon, Eqs. (1)–(5) were integrated numerically in the (X, Y, Z) reference frame, considering a propagation time of 10

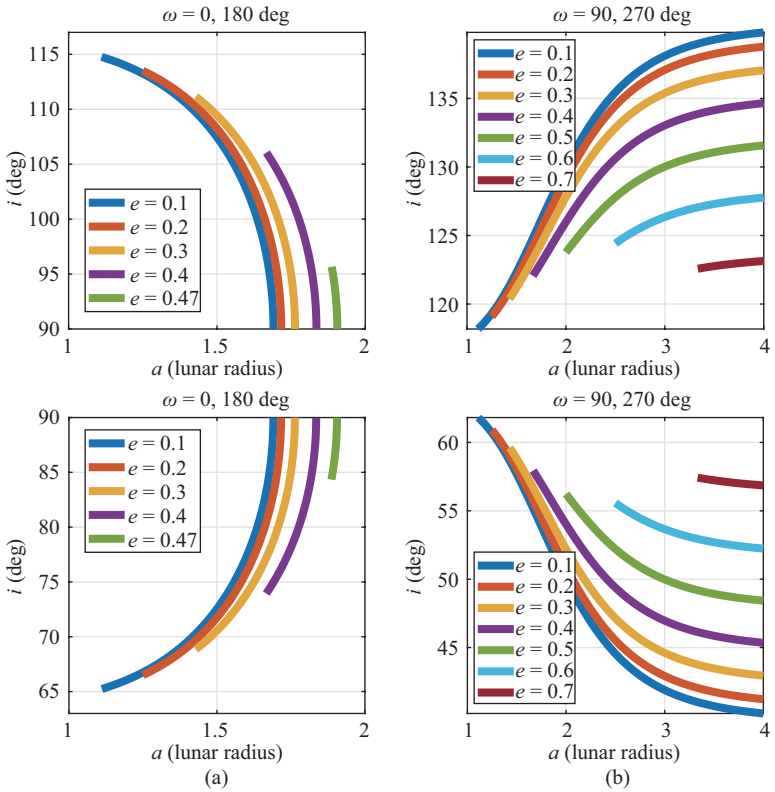

Fig. 4 Frozen orbits around the Moon at $\omega = 0$ or 180 deg (a) and at $\omega = 90$ or 270 deg (b), assuming the Earth's relative orbit as laying on the Moon's equatorial plane.

terrestrial years (the real obliquity of the Earth, 6.69 deg, is now considered). In general, the analysis has proven that the solutions presented in Fig. 4 are associated with a longer impact time. For this reason, such solutions are hereafter referred to as long-lifetime orbits around the Moon.

As an example, Fig. 5 shows, on plane (a, i), the results obtained with the following initial conditions: $e = 0.1$, $\omega = 0$, and several values of $\Omega = \{0, 90, 180, 270\}$ deg. The blue regions correspond to the non-collision conditions (over a timespan of 10 years). In particular, the plots highlight that the dependence on Ω is rather weak, and the non-collision condition is achieved in a region bounded by the related curve shown in Fig. 4(a) (i.e., the family at $\omega = 0$ or 180 deg and $e = 0.1$). In addition, the non-collision condition is obtained for inclination values smaller than 63.43 deg and greater than 116.57 deg (critical inclinations at only J_2). In fact, at mid and low inclinations, the variation in eccentricity correlated with the third-body effect is weaker [1–5].

Figure 6 shows the same outcomes but starting from the following initial conditions: $e = 0.6$, $\omega = 90$ deg, $\Omega = \{0, 90, 180, 270\}$ deg. This figure highlights how the dependence on Ω is more marked in this case, even though the non-collision condition is still achieved in correspondence to points belonging to the related solution shown in Fig. 4(b) (family at $\omega = 90$ or 270 deg and $e = 0.6$).

3.2 Numerical simulations in the non-averaged model

In Section 3.1, the perturbations associated with the Sun and the higher harmonics of the gravitational field of the Moon have been neglected, and the disturbing function related to the Earth has been truncated at the second order (quadrupole approximation). Moreover,

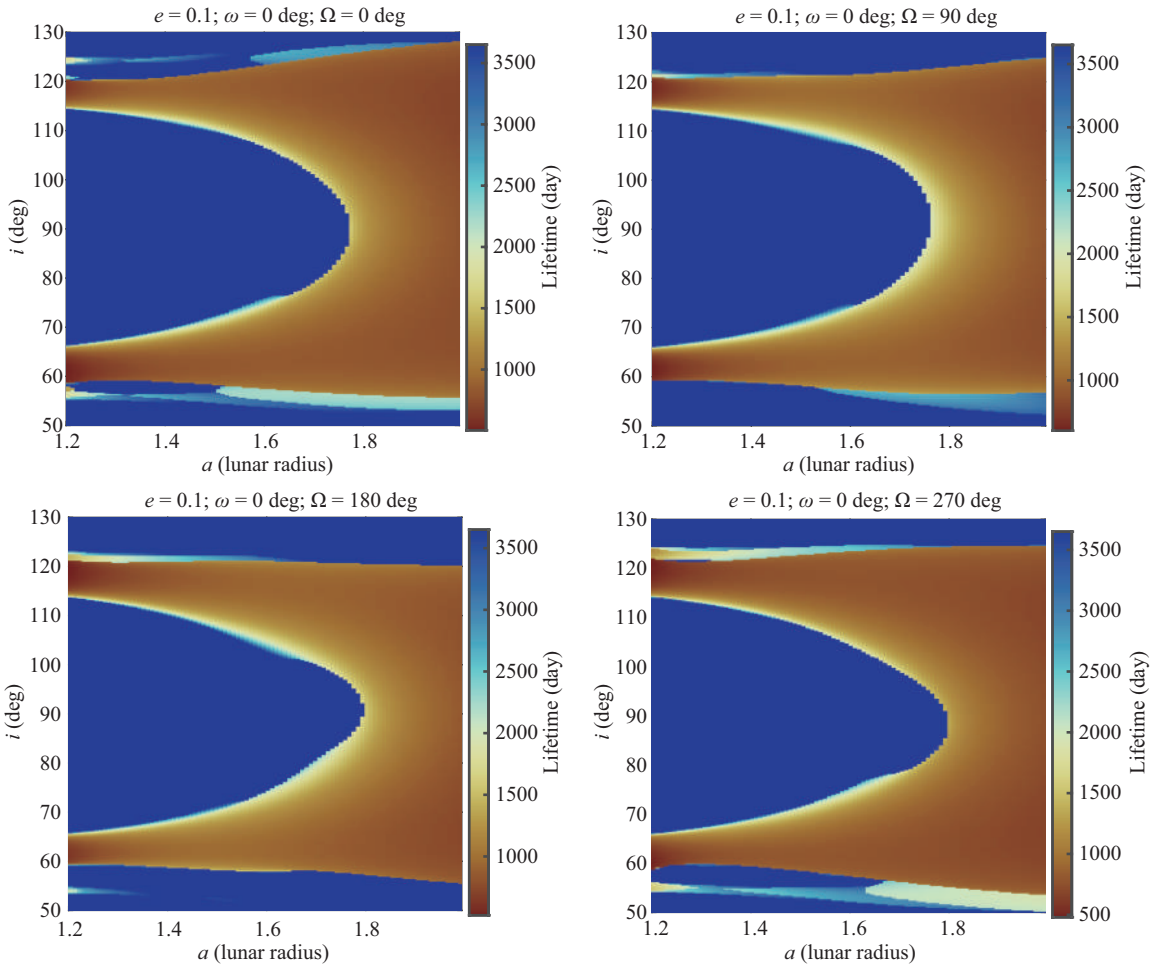

Fig. 5 Lifetime for a Moon-based mission scenario, starting from $e = 0.1$; $\omega = 0$ deg; $\Omega = \{0, 90, 180, 270\}$ deg.

although the MET allows, in general, accurate predictions about the evolution of the mean orbit elements of the probe orbit, the osculating orbit elements can present small deviations with respect to them [4, 14]. For these reasons, a numerical analysis was performed on the long-lifetime orbits proposed in this study. In the analysis, the gravitational attractions of both the Earth and the Sun have been considered, evaluating their positions in accordance with the ephemeris model JPL DE405 [26]. In addition, for the Moon, the LP165p (Lunar Prospector 165p) gravitational model has been implemented up to degree and order 80×80 [20], without performing any averaging procedure (non-averaged full model).

In general, the results of the numerical simulations have proved to be close to the ones obtained in the averaged model. As examples, Figs. 7 and 8 illustrate the temporal evolution of the orbital elements related to two long-lifetime solutions shown in Fig. 4(a) ($\omega = 0$, 180 deg), whereas Figs. 9 and 10 show the evolution of the orbital elements of two long-lifetime solutions presented in Fig. 4(b) ($\omega = 90$ deg; similar results were obtained for the same orbit but with $\omega = 270$ deg). The corresponding

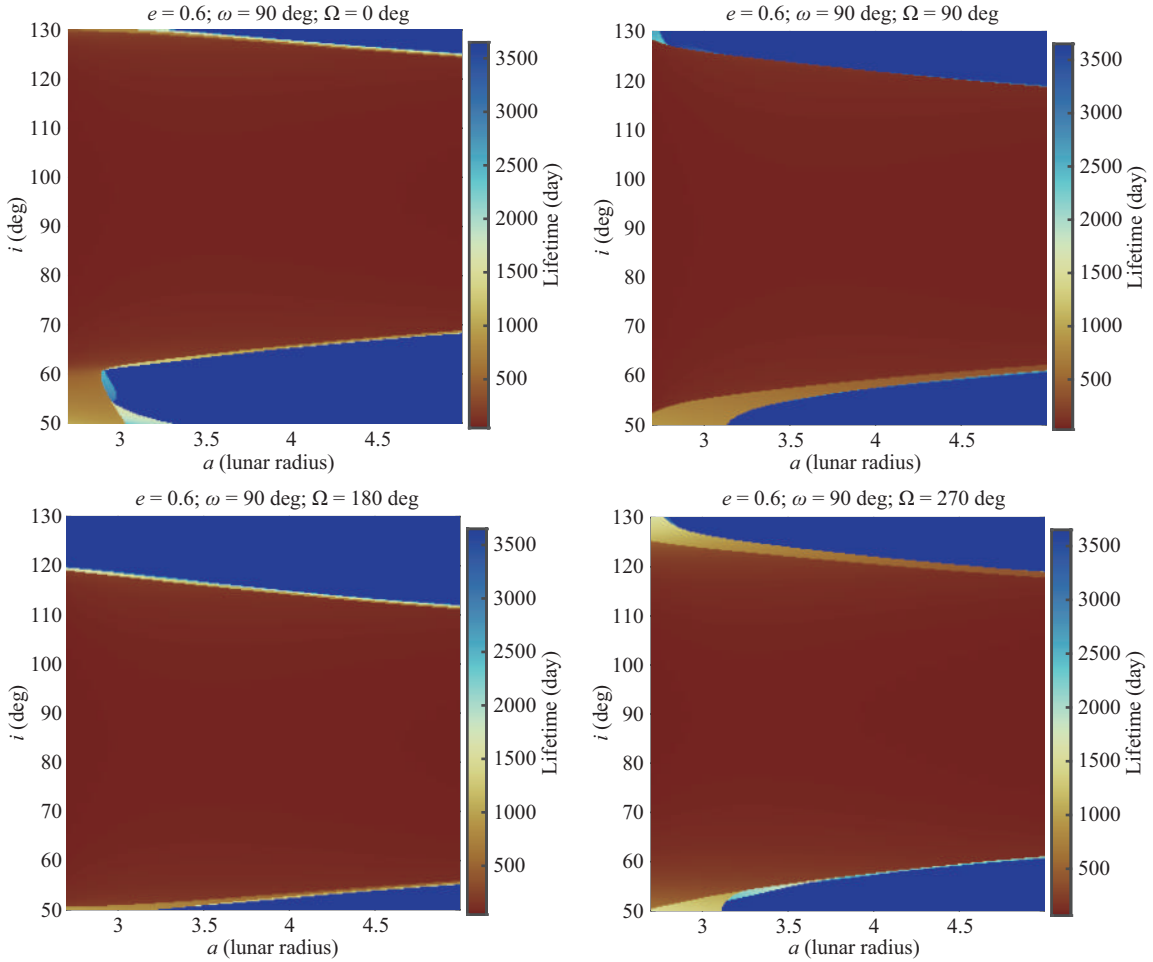

Fig. 6 Lifetime for a Moon-based mission scenario, starting from $e = 0.6$; $\omega = 90$; $\Omega = \{0, 90, 180, 270\}$ deg.

Table 2 Nominal values of the orbit elements of the spacecraft for four proposed solutions (note that the RAAN also refers to the probe orbit)

Keplerian orbital period (h)	a (km)	e	i (deg)	RAAN	ω (deg)	f	Figure
3	2437.684	0.1	69.61	0	0	0	Fig. 7
~3.97	2938.224	0.1	90.00	0	180	0	Fig. 8
12	6142.578	0.6	52.66	0	90	0	Fig. 9
14	6807.409	0.6	52.29	0	90	0	Fig. 10

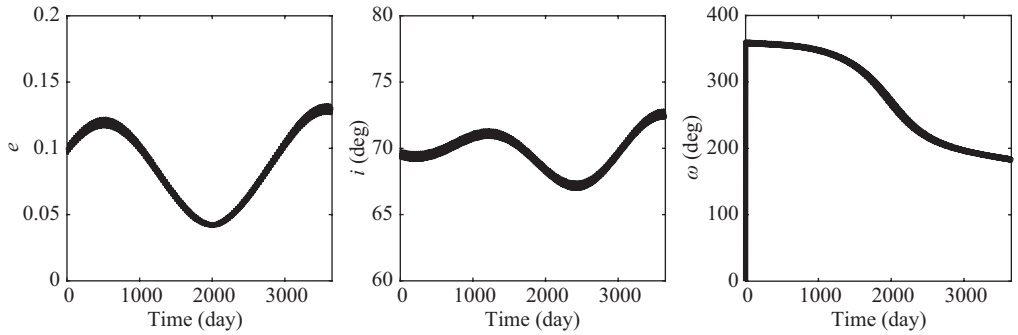

Fig. 7 Time variation of the orbit elements for a proposed orbit with a period of 3 h. The initial conditions are reported in Table 2.

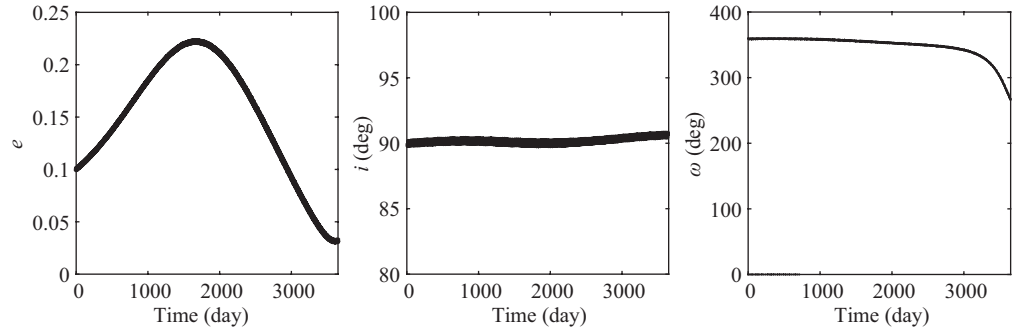

Fig. 8 Time variation of the orbit elements for a proposed orbit with a period of 3.97 h. The initial conditions are reported in Table 2.

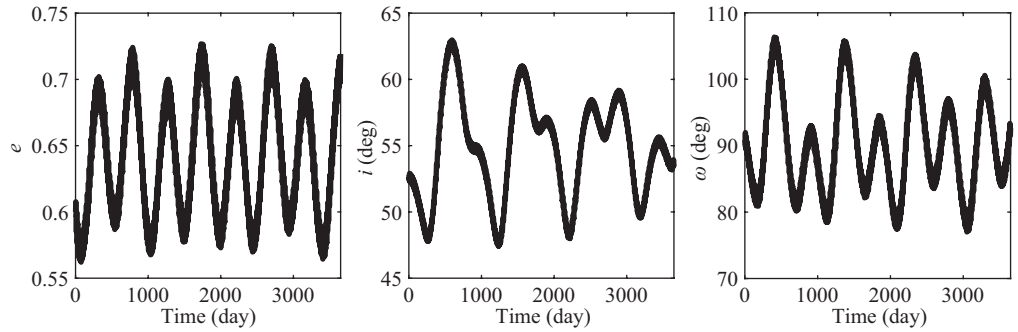

Fig. 9 Time variation of the orbit elements for a proposed orbit with a period of 12 h. The initial conditions are reported in Table 2.

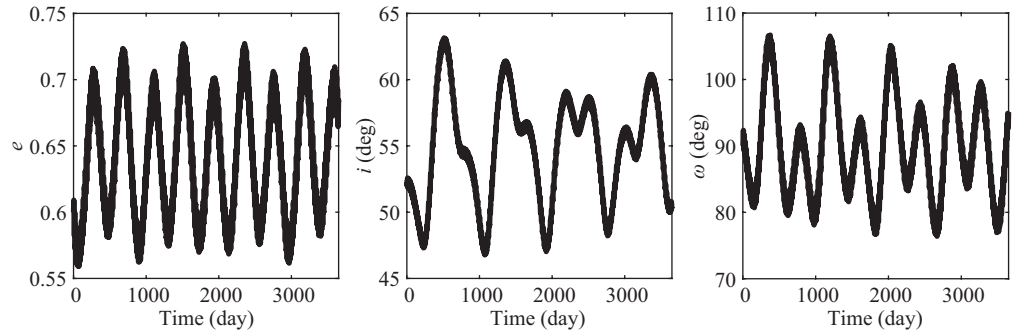

Fig. 10 Time variation of the orbit elements for a proposed orbit with a period of 14 h. The initial conditions are reported in Table 2.

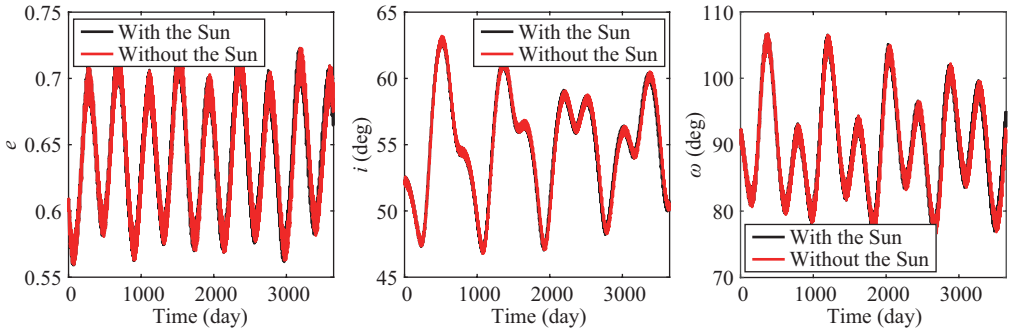

Fig. 11 Comparison between the time variations of the orbit elements for the orbit of Fig. 10, with and without the gravitational attraction of the Sun.

initial conditions are listed in Table 2, where f denotes the true anomaly of the probe. In particular, the two solutions at $\omega = 90$ deg were selected based on the general architecture proposed in Ref. [10], and shown in Fig. 1. Note that in the figures, the mean values of e, i, and ω remain quasi-constant on average.

To conclude the analysis, Fig. 11 shows the evolution of the orbital elements of the solution in Fig. 10, removing the gravitational influence of the Sun. As the evidence shows, the attraction of the Sun does not have a significant effect.

4 Conclusions

Two families of long-lifetime elliptical orbits have been proposed for probes orbiting the Moon. One family is characterized by an argument of the pericenter of the probe orbit equal to 0 or 180 deg and an eccentricity smaller than 0.47876, and the other by an argument of the pericenter equal to 90 or 270 deg. At mid and high altitudes, the other orbit elements of these solutions can be set to meet the requirements of a system for lunar telecommunication and navigation services. Examples characterized by a time to impact longer than 10 terrestrial years have been presented. Potential applications for future missions related to this planetary satellite follow.

Funding note

Open access funding provided by Istituto Nazionale di Astrofisica within the CRUI-CARE Agreement.

Acknowledgements

M. Cinelli was supported by the G4S_2.0 project, developed under the auspices of the Italian Space Agency (ASI) within the framework of the Bando Premiale CI-COT-2018-085, with the co-participation of the Italian Institute for Astrophysics (INAF) and the Politecnico di Torino (POLITO).

Declaration of competing interest

The authors have no competing interests to declare that are relevant to the content of this article. The authors Emiliano Ortore, Alessandro A. Quarta, and Christian Circi are the Associate Editors of this journal.

References

[1] Scheeres, D. J., Guman, M. D., Villac, B. F. Stability analysis of planetary satellite orbiters: Application to the Europa orbiter. *Journal of Guidance, Control, and Dynamics*, **2001**, 24(4): 778–787.

[2] Broucke, R. A. Long-term third-body effects via double averaging. *Journal of Guidance, Control, and Dynamics*, **2003**, 26(1): 27–32.

[3] Russell, R. P., Brinckerhoff, A. T. Circulating eccentric orbits around planetary moons. *Journal of Guidance, Control, and Dynamics*, **2009**, 32(2): 424–436.

[4] Paskowitz, M. E., Scheeres, D. J. Design of science orbits about planetary satellites: Application to Europa. *Journal of Guidance, Control, and Dynamics*, **2006**, 29(5): 1147–1158.

[5] Cinelli, M., Ortore, E., Circi, C. Long lifetime orbits for the observation of Europa. *Journal of Guidance, Control, and Dynamics*, **2018**, 42(1): 123–135.

[6] Ortore, E., Cinelli, M., Circi, C. Optimal initial conditions for science orbits around Ganymede. *Advances in Space Research*, **2023**, 72(8): 3308–3320.

[7] Smith, M., Craig, D., Herrmann, N. B., Mahoney, E., Krezel, J., McIntyre, N., Goodliff, K. The Artemis program: An overview of NASA's activities to return

humans to the Moon. In: Proceedings of the IEEE Aerospace Conference, **2020**: 1–10.

[8] Lu, Y., Yang, Y.-K., Li, X., Zhu, Z.-Y., Li, H.-T., Dong, G.-L. Lunar high frozen orbit relay satellite constellation and its deployment and maintenance. In: *China Satellite Navigation Conference (CSNC) 2012 Proceedings. Lecture Notes in Electrical Engineering, Vol. 159*. Sun, J., Liu, J., Yang, Y., Fan, S. Eds. Springer Berlin Heidelberg, **2012**: 257–266.

[9] Zhou, W., Gao, S., Liu, D., Zhang, X., Ma, J., Yu, D. Orbit design for lunar polar region exploration. *Journal of Deep Space Exploration*, **2020**, 7(3): 248–254. (in Chinese)

[10] Tai, W., Kim, I., Moon, S., Kim, D. Y., Cheung, K. M., Koo, C. H., Schier, J., Rew, D. Y. The lunar space communications architecture: Beyond the NASA–KARI study. In: *Space Operations: Contributions from the Global Community*. Cruzen, C., Schmidhuber, M., Lee, Y., Kim, B. Eds. Springer Cham, **2017**: 149–174.

[11] Cosby M, Tai W, *et al*. The future lunar communications architecture. Technical Report. Washington, D.C., USA: Interagency Operations Advisory Group, **2022**. Available at https://www.ioag.org/Public%20Documents/Lunar%20communications%20architecture%20study%20report%20FINAL%20v1.3.pdf

[12] Coffey, S. L., Deprit, A., Deprit, E. Frozen orbits for satellites close to an Earth-like planet. *Celestial Mechanics and Dynamical Astronomy*, **1994**, 59(1): 37–72.

[13] Ma, Y., He, Y., Xu., Zheng, Y. Global searches of frozen orbits around an oblate Earth-like planet. *Astrodynamics*, **2022**, 6(3): 249–268.

[14] Nie, T., Gurfil, P. Lunar frozen orbits revisited. *Celestial Mechanics and Dynamical Astronomy*, **2018**, 130: 61.

[15] Condoleo, E., Cinelli, M., Ortore, E., Circi, C. Frozen orbits with equatorial perturbing bodies: The case of Ganymede, Callisto, and Titan. *Journal of Guidance, Control, and Dynamics*, **2016**, 39(10): 2264–2272.

[16] Kozai, Y. The motion of a close Earth satellite. *The Astronomical Journal*, **1959**, 64: 367.

[17] Merson, R. H. The motion of a satellite in an axi-symmetric gravitational field. *Geophysical Journal International*, **1961**, 4(Supplement_1): 17–52.

[18] De Almeida Prado, A. F. B. Third-body perturbation in orbits around natural satellites. *Journal of Guidance, Control, and Dynamics*, **2003**, 26(1): 33–40.

[19] Lang, K. R. *The Cambridge Guide to the Solar System*, 2nd edn. Cambridge, UK: Cambridge University Press, **2011**.

[20] Konopliv, A. S., Asmar, S. W., Carranza, E., Sjogren, W. L., Yuan, D. N. Recent gravity models as a result of the lunar prospector mission. *Icarus*, **2001**, 150(1): 1–18.

[21] Cinelli, M., Lei, H. L., Ortore, E., Circi, C. Probe lifetime around natural satellites with obliquity. *Astrodynamics*, **2022**, 6(4): 429–439.

[22] Rosengren, A. J., Scheeres, D. J. Long-term dynamics of high area-to-mass ratio objects in high-Earth orbit. *Advances in Space Research*, **2013**, 52(8): 1545–1560.

[23] Kozai, Y. Secular perturbations of asteroids with high inclination and eccentricity. *The Astronomical Journal*, **1962**, 67: 591–598.

[24] Lidov, M. L. The evolution of orbits of artificial satellites of planets under the action of gravitational perturbations of external bodies. *Planetary and Space Science*, **1962**, 9(10): 719–759.

[25] Naoz, S. The eccentric Kozai–Lidov effect and its applications. *Annual Review of Astronomy and Astrophysics*, **2016**, 54: 441–489.

[26] Standish, E. JPL planetary and lunar ephemerides, DE405/LE405. JPL IOM 312. Technical Report, No. F-98-048, **1998**.

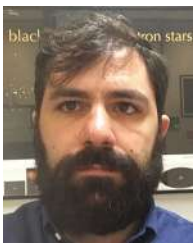

Marco Cinelli received his Ph.D. degree in 2017 from Sapienza University of Rome, Italy. He is a research fellow at the Istituto di Astrofisica e Planetologia Spaziali (IAPS) of the Italian National Institute for Astrophysics (INAF) in Rome. He is currently involved in the GALILEO for Science project (G4S) funded by the Italian Space Agency (ASI) and aims to perform a set of measurements in the field of fundamental physics with the two Galileo satellites DORESA and MILENA. He is adjunct professor at the Universitas Mercatorum of Rome, Italy. E-mail: marco.cinelli@uniroma2.it

Emiliano Ortore graduated in aerospace engineering (M.S. degree) and in astronautical engineering and pursued his Ph.D. degree in aerospace engineering at Sapienza University of Rome, Italy. Since 2004, he has been working as a researcher at Sapienza University of Rome. Research fields: celestial mechanics; astrodynamics, including science orbits around planets, moons, and asteroids; orbits and satellite constellations for applications of remote sensing, telecommunication, and navigation. E-mail: emiliano.ortore@uniroma1.it

Giovanni Mengali received his Doctor of Engineer degree in aeronautical engineering in 1989 from the University of Pisa, Italy. Since 1990, he has been with the Department of Aerospace Engineering (now Department of Civil and Industrial Engineering) of the University of Pisa, first as a Ph.D. student, then as an assistant and an associate professor. Currently, he is professor of spaceflight mechanics. His main research areas include spacecraft mission analysis, trajectory optimization, solar sails, electric sails, and aircraft flight dynamics and control. E-mail: g.mengali@ing.unipi.it

Alessandro A. Quarta received his Ph.D. degree in aerospace engineering from the University of Pisa in 2005 and he is currently a professor of flight mechanics at the Department of Civil and Industrial Engineering of this university. His main research areas include spaceflight simulation, spacecraft mission analysis and design, low-thrust trajectory optimization, and solar sail and E-sail dynamics and control. E-mail: a.quarta@ing.unipi.it

Christian Circi is currently an associate professor in flight mechanics at the Department of Astronautical, Electrical, and Energy Engineering, Sapienza University of Rome, Italy. He received his M.S. degree in aeronautical engineering and aerospace engineering, and his Ph.D. degree in aerospace engineering at Sapienza University of Rome. He worked as a researcher at the Grupo de Mecanica of Vuelo-Madrid (GMV) and a research assistant at the Department of Aerospace Engineering. He is a lecturer in "Interplanetary Trajectories" and "Flight Mechanics of Launcher" in the master degree course of space and astronautical engineering at this university. His principal research fields are third-body and solar perturbations, interplanetary and lunar trajectories, solar sails, orbits for planetary observation, and the ascent trajectory of launcher. He is associate editor for *Aerospace Science and Technology*, *International Journal of Aerospace Engineering*, and *Astrodynamics*. E-mail: christian.circi@uniroma1.it